A condensed modal functional for identifying equivalent constitutive properties of an assembled induction motor

Guillaume Mogenier, Thouraya Nouri-Baranger, Lionel Durantay, Nicolas Barras

**Proceedings of the ASME 2009 International Design Engineering Technical Conferences &
Computers and Information in Engineering Conference
IDETC/CIE 2009
August 30 - September 2, 2009, San Diego, California, USA**

DETC2009-86960

A CONDENSED MODAL FUNCTIONAL FOR IDENTIFYING EQUIVALENT CONSTITUTIVE PROPERTIES OF AN ASSEMBLED INDUCTION MOTOR

Guillaume Mogenier
Universit de Lyon, CNRS
INSA-Lyon, LaMCoS UMR5259,
Villeurbanne, F-69621, France
guillaume.mogenier@insa-lyon.fr

Thouraya Nouri Baranger
Second Coauthor
Universit de Lyon 1
Villeurbanne, F-69622, France
Université de Lyon, CNRS
INSA-Lyon, LaMCoS UMR5259
Villeurbanne, F-69621, France
thouraya.baranger@insa-lyon.fr

Rgis Dufour
Third Coauthor
Universit de Lyon, CNRS
INSA-Lyon, LaMCoS UMR5259
Villeurbanne, F-69621, France
regis.dufour@insa-lyon.fr

Lionel Durantay
Fourth Coauthor
Converteam SAS
Motors Division
54250 Champigneulles, France
lionel.durantay@converteam.com

Nicolas Barras
Fifth Coauthor
Converteam SAS
Motors Division
54250 Champigneulles, France
nicolas.barras@insa-lyon.fr

ABSTRACT

In order to predict the lateral rotordynamics of a high speed induction motor, an optimization procedure is proposed for identifying the equivalent constitutive properties especially those of the magnetic core: an assembly of lamination stack, tie rods and short-circuit rods. Modal parameters predicted by a finite element (FE) branched model based mainly on beam elements, and measured on an induction motor are included in an original energy functional. The minimization of this functional by using the Levenberg-Marquardt algorithm permits extracting the equivalent constitutive properties of the lamination stack.

NOMENCLATURE

c_j	The j^{th} projection coordinate of an eigenvector partial derivative in the modal basis.
d_i	Descent direction at iteration i.
d_{ti}^{in}	Equivalent inlet diameter of the tie rods, m.
d_{ti}^{out}	Equivalent outlet diameter of the tie rods, m.
E	Young modulus, $N \cdot m^{-2}$.
E_0	Young modulus value at iteration 0, $N \cdot m^{-2}$.
f	Global energy functional.
G	Shear modulus, $N \cdot m^{-2}$.
G_0	Shear modulus value at iteration 0, $N \cdot m^{-2}$.
H_i	Approximate Hessian matrix of f at iteration i.
I	Identity matrix of rank n.
I_{ti}	Second moment of area of the tie rods, m^4.
J	Jacobian matrix of the error estimation $\mathscr{E}$.
K	Global stiffness matrix.
K_{cc}	Global stiffness matrix partition related to the boundary degrees of freedom.
K_{ci}	Global stiffness matrix partition related to the coupling between the interior and boundary degrees of freedom.
K_f	Global structural stiffness matrix.
K_{ic}	Global stiffness matrix partition related to the coupling

between the interior and boundary degrees of freedom.

K_{ii} Global stiffness matrix partition related to the interior degrees of freedom.

K_P Global stress stiffening matrix.

K_r Condensed global stiffness matrix.

m Number of eigen-elements.

M Global mass matrix.

M_{cc} Global mass matrix partition related to the boundary degrees of freedom.

M_{ci} Global mass matrix partition related to the coupling between the interior and boundary degrees of freedom.

M_{ic} Global mass matrix partition related to the coupling between the interior and boundary degrees of freedom.

M_{ii} Global mass matrix partition related to the interior degrees of freedom.

M_r Condensed global mass matrix.

M_R Global mass matrix due to the cross-section rotation.

M_T Global mass matrix due to the cross-section translation.

n Number of optimization variables.

n_c Number of boundary degrees of freedom.

n_i Number of interior degrees of freedom.

p Optimization variable index.

q Modal generalized coordinates.

R_k The k^{th} Rayleigh quotient, $rad^2.s^{-2}$.

R_k^* The k^{th} hybrid Rayleigh quotient, $rad^2.s^{-2}$.

S_{ti} The whole surface of the tie rods, m^2.

T Matrix assuming a condensed global matrix.

x Optimization variables.

x^i The i^{th} iterate of the optimization algorithm.

x_p The p^{th} optimization variable.

x^0 Optimization variable values at iteration 0.

δ Displacements of the degrees of freedom, m.

δ_c Displacements of the boundary degrees of freedom, m.

δ_i Displacements of the interior degrees of freedom, m.

$\mathscr{E}_k$ Error estimation between the k^{th} predicted and measured modal quantities.

λ_k The k^{th} eigenvalue of the condensed FE model, $rad^2.s^{-2}$.

$\hat{\lambda}_k$ The k^{th} eigenvalue of the total FE model, $rad^2.s^{-2}$.

λ_k^n The k^{th} eigenvalue of the constrained FE model, $rad^2.s^{-2}$.

ρ_i Descent step at iteration i.

μ_0 Marquardt's parameter at iteration 0.

μ_i Marquardt's parameter at iteration i.

υ Poisson ratio.

φ_k The k^{th} measured mode shape.

$\widetilde{\varphi}_k$ The k^{th} mode shape of the condensed FE model.

$\hat{\varphi}_k$ The k^{th} mode shape of the FE model.

φ^c Matrix of constrained modes.

${}^c\widetilde{\varphi}_k$ The k^{th} modal shape of the boundary degrees of freedom.

φ^n Matrix of normal modes.

φ_k^* The vector containing the k^{th} measured modal shape and the modal generalized coordinates q.

Ψ Transformation matrix.

ω_k The k^{th} measured natural angular frequency, $rad.s^{-1}$.

$\hat{\omega}_k$ The k^{th} predicted natural angular frequency, $rad.s^{-1}$.

∇ Differential operator.

INTRODUCTION

This paper focuses on squirrel cage induction motors, called *MGV* (Moteur Grande Vitesse), in the 3 to 30 *MW* range from 6000 to 18000 *rpm* used for critical applications, especially motocompressors, in the oil and gas industry. As shown in Fig. 1, *MGV* rotors are mainly composed of two steel shaft ends and full depth laminations held together by steel tie rods. The squirrel cage consists of copper short-circuit rods distributed at the periphery of the core and linked to two bronze alloy rings placed at both ends of the stack. The stack and the two rings are tightened by the tie rods, also distributed at the periphery of the core and screwed in the ends of the two shaft ends.

The problem of modeling the magnetic core and the stacks of full depth laminations has been given little attention in scientific papers. Refs. [1] and [2] suggested a homogenized bending rigidity for the entire magnetic core cross-section by adding the bending rigidity of each cross-section component. Ref. [3] deals with a stiff shaft design for a squirrel cage rotor but the bending rigidity of the magnetic core is not described. However, many authors have attempted to predict the dynamic behavior of induction machine rotors with laminated rotor core mounted on a solid shaft, *i.e.* laminations with a central hole. The stiffening effects of the laminated core are not easy to assess and often require identification via modal testing. Ref. [4] assesses the influence of leading parameters, such as stack length, on the natural frequencies of a high-speed permanent magnet brushless machine by using a three dimensional FE model. Ref. [5] presents the advantages of a branched model for a laminated rotor. The laminations are considered as several annular rings subsets linked altogether by elastic connections. Moreover, the subsets are elastically connected to the shaft. Ref. [6] considers an equivalent Young modulus for the stack and uses a branched beam model for the magnetic core. The authors of many papers have dealt with a coefficient called stacking factor which modifies the value of the mass of lamination stack [7,8]. Also, its weak Young modulus is due resin or varnish layers on the interfaces between consecutive laminations [9]. Ref. [5] considers the lamination stack as an orthotropic material whose elastic strain-stress relation taking into account the lamination material and the mean flexibilities (shear and compressive) of the lamination interfaces. Ref. [10] shows that the lamination pressure has considerable influence on the lateral natural frequencies of a rotor. An equivalent diameter and lumped masses are considered for modeling the entire magnetic core.

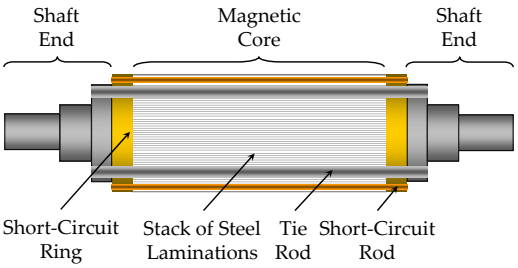

Figure 1. DIAGRAM OF A SQUIRREL CAGE INDUCTION ROTOR.

In identification procedures, an optimization algorithm is used so that optimization parameters of a FE model make predicted data tend toward target values, *i.e.* measured data. Such algorithms can use modal data for updating and then identifying the FE model parameters. Modal error functions are defined to quantify the difference between predicted and measured natural frequencies and mode shapes. Thus, Ref. [11] uses a common modal error function based on natural frequencies in order to identify the properties of laminated composite plates. Ref. [12] proposes two original modal error functions based on the diagonal and extra-diagonal terms of the modal assurance criterion (MAC) matrix. Ref. [13] uses a more classical modal error function, based on the difference between the components of predicted and measured mode shapes, to identify material parameters of a concrete dam. These functions are combined as a least square functional whose minimization requires its derivatives, with respect to the optimization parameters, that depend on eigen-element derivatives. Eigenvalue derivatives are obtained from the relationship given by [14] whereas eigenvector derivatives can be computed by using approximate or exact methods [15]. Ref. [16] compares different algorithms regarding this point.

In this paper, a FE model of an induction rotor is presented with particular attention given to the modeling of the magnetic core. A branched model is then proposed to model the tie rods independently of the lamination stack. It mainly uses beam elements in order to have few degrees of freedom (dof) and to predict for instance transient responses. Given certain assumptions, tie and short-circuit rods can be modeled by using only Timoshenko's in-plane beam elements. Even if a beam based model is used, the constitutive properties of the stack are defined such that the shear and the Young moduli are independent for taking into account its orthotropic properties [5]. Thus, the lateral dynamic behavior of the stack is identified by performing an experimental modal analysis. The identification strategy consists in minimizing the difference between the measured and the predicted modal data provided by the FE branched model. This difference is quantified by an energy functional coupled with the Craig and Bampton reduction in order to make predicted and measured mode shapes' size compatible [17]. Moreover, the condensed model retains local modes of the complete FE model. This functional, inspired by [18], allows homogeneous terms between each mode and especially provides, for each mode, a unique term obtained by combining the natural frequency and its associated mode shape. The functional minimization is performed by using the Levenberg-Marquardt algorithm which provides a set of constitutive properties for the lamination stack. Consequently, this requires eigen-element derivatives computed analytically to ensure that the optimization algorithm is more efficient.

FINITE ELEMENT MODEL

The FE model of the induction rotor is based on the structural dynamics theory described in [19]. The expression of the global stiffness matrix is as follows:

$$K = K_f + K_P, \tag{1}$$

where K_f is the structural stiffness matrix and K_P is the stress stiffening matrix if an axial prestressing force acts on the beam FE [20]. The global mass matrix can be written as:

$$M = M_T + M_R, \tag{2}$$

where M_T and M_R are due to the translation and the rotatory inertia of the cross-section respectively, the latter being classically neglected for slender structures. Shear strain and rotatory inertia are taken into account in the Timoshenko's in-plane beam FE containing two dof per node: one translation and one rotation. A shear correction factor dependent on the shape of the cross-section is used as in [21].

Free-free boundary conditions are taken into account by adding low stiffness springs ($10N \cdot m^{-1}$) at each boundary node. Disks and landing rings are considered as lumped masses. For identifying stiffness parameters relative to the lamination stack, specific assumptions have to be considered to model the tie and the short-circuit rods. The short-circuit rods can be modeled as beams whose neutral axes coincide with the neutral axis of the magnetic core. Indeed, these rods are built in the middle of the magnetic core thanks to screws and their ends are able to slide in the short-circuit rings as shown in Fig. 2. Thus, each FE of the discretized magnetic core is connected to two consecutive nodes;its elementary matrices being the sum of those related to the short-circuit rods and the lamination stack. Furthermore, he tie rods are modeled as an equivalent hollow cylinder clamped

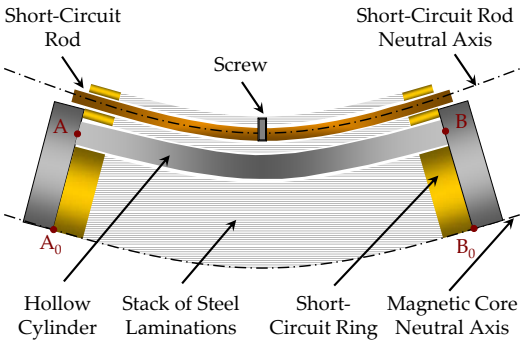

Figure 2. SHORT-CURCUIT ROD IN BENDING - KINEMATIC ASSUMPTION.

at nodes A_0 and B_0 (see Fig. 2) to form a FE branched model. Therefore, the tie rods are independently modeled of the lamination stack. Let d_{ti}^{out} and d_{ti}^{in} be its outer and inner diameters respectively and simply calculated by considering the surface S_{ti} and second moment of area I_{ti} of the tie rods:

$$d_{ti}^{out} = \left(\frac{8I_{ti}}{S_{ti}} + \frac{2S_{ti}}{\pi}\right)^{\frac{1}{2}}, d_{ti}^{in} = \left(\frac{8I_{ti}}{S_{ti}} - \frac{2S_{ti}}{\pi}\right)^{\frac{1}{2}}. \quad (3)$$

The screwing torque ensures the stress stiffening in the tie rods and the prestressing in the lamination stack. The stress stiffening effect is taken into account by the K_P matrix only for the hollow cylinder. The measuring is performed on the assembled structure therefore identified parameters implicitly take into account the prestressing. Since the short-circuit rings, the lamination stack and the shaft ends connected to each short-circuit rings are drilled at their periphery for the short-circuit rods and tie rods, Eqn. (3) is also used for the modeling of these elements' cross-section.

OPTIMIZATION STRATEGY

The equivalent constitutive properties of the lamination stack are denoted as $x \in \mathbb{R}^n$ so that $\{x_p\}_{p=1\ldots n}$. The optimization parameters, from the following doublet:

$$\{E, G\}, \quad (4)$$

where E, G are the Young and shear moduli respectively are independent for modeling anisotropy, as described in [5]. The optimization parameter number is then equal to two, *i.e.* $(n = 2)$. The identification strategy consists in minimizing the difference between predicted and measured modal data.

Condensed Modal Functional

An optimization algorithm is used so that optimization parameters of the FE branched model make predicted data tend toward target values. Let x^i be the vector of optimization parameters x at iteration i. Let us assume that all variables of the FE model depend on x^i. Let $\hat{\omega}_k$ and ω_k be the predicted and measured natural frequencies respectively. Let $\hat{\varphi}_k$ and φ_k be their associate mode shapes. They have to be projected in the same spatial basis. The symmetric eigenvalue equations of an undamped system in structural dynamics can be defined as follows:

$$\left(K - \hat{\lambda}_k M\right)\hat{\varphi}_k = 0, \hat{\lambda}_k = \hat{\omega}_k^2, (k = 1, \ldots, m), \quad (5)$$

where m is the number of eigen-elements. The same problem can be written in a more compact form:

$$R_k - \hat{\omega}_k^2 = 0, \quad (6)$$

where R_k denotes the Rayleigh quotient defined as the ratio of the strain energy over the kinetic energy of the k^{th} mode shape:

$$R_k = \frac{\varphi_k^t K \hat{\varphi}_k}{\varphi_k^t M \hat{\varphi}_k}. \quad (7)$$

In this way, an exact correlation between predicted and measured natural frequencies and mode shapes leads to, for each mode k:

$$\hat{\varphi}_k = \varphi_k, \hat{\omega}_k^2 = \omega_k^2. \quad (8)$$

By taking account of Eqn. (8), Eqn. (6) can be written in adimensional terms:

$$1 - \frac{1}{\omega_k^2} \cdot \frac{\varphi_k^t K \hat{\varphi}_k}{\varphi_k^t M \hat{\varphi}_k} = 0. \quad (9)$$

However, an exact correlation never appears in real cases. Thus, we propose to quantify the difference between predicted and measured modal data with the left part of Eqn. (9) such as:

$$\mathscr{E}_k\left(\mathrm{x}^{\mathrm{i}}\right) = 1 - \frac{1}{\omega_k^2} \cdot \frac{\varphi_k^t K \hat{\varphi}_k}{\varphi_k^t M \hat{\varphi}_k}. \quad (10)$$

Nevertheless, the problem is that predicted and measured mode shapes $\widetilde{\varphi}_k$ and φ_k do not have the same size. Indeed, the predicted mode shapes are composed of two kinds of dof, *i.e.* lateral deflections and in-plane rotations whereas the experimental

mode shapes are only composed of the measured lateral deflections. So, the use of a reduction method is suggested in order to make predicted and measured mode shapes' size compatible. By considering the equivalent hollow cylinder and the rotor as two substructures, the Craig and Bampton reduction is an appropriate method to condensed the FE branched model. Moreover, by retaining normal modes, this method provides local modes such as tie rods modes. The boundary dof δ_c, of size $[n_c \times 1]$, are then chosen to be the lateral deflections of the rotor (measured values) whereas the interior dof δ_i, of size $[n_i \times 1]$, to be the lateral deflections of the equivalent hollow cylinder (tie rods) and the all in-plane rotations [17]. The δ vector of the FE branched model dof can be partitioned as shown in Eqn. (11):

$$\{\delta\} = \langle \delta_i, \delta_c \rangle^t . \tag{11}$$

The global mass and stiffness matrices of Eqn. (5) can be expressed in term of matrix partitions such as:

$$K = \begin{bmatrix} K_{ii} & K_{ic} \\ K_{ci} & K_{cc} \end{bmatrix}, M = \begin{bmatrix} M_{ii} & M_{ic} \\ M_{ci} & M_{cc} \end{bmatrix}. \tag{12}$$

The transformation matrix ψ can be written as follows:

$$\psi = \begin{bmatrix} \varphi^c & \varphi^n \\ I & 0 \end{bmatrix}, \tag{13}$$

where I is the identity matrix of size $[n_c \times n_c]$, φ^c means the constrained modes obtained by setting the forces at all interior dof equal to zero:

$$\varphi^c = -K_{ii}^{-1} \cdot K_{ic}, \tag{14}$$

and φ^n denotes the normal modes obtained by considering all the boundary dof as constrained:

$$(K_{ii} - \lambda_k^n M_{ii})\, \varphi_k^n = 0, \, (k = 1, \ldots, n_i), \tag{15}$$

where λ_k^n is the k^{th} eigenvalue of the FE model with boundary constrained. The δ vector can then be written as:

$$\{\delta\} = \psi \cdot \begin{Bmatrix} \delta_c \\ q \end{Bmatrix}, \tag{16}$$

where q are modal generalized coordinates associated with the eigenvectors contained in φ^n. The mass and stiffness matrices can then be written in condensed forms such as:

$$\begin{array}{l} M_r = \psi^t \cdot M \cdot \psi \\ K_r = \psi^t \cdot K \cdot \psi \end{array}. \tag{17}$$

Thus, the symmetric eigenvalue equations of the condensed undamped system is written as follows:

$$(K_r - \lambda_k M_r)\, \widetilde{\varphi}_k = 0, \lambda_k = \tilde{\omega}_k^2, \, (k = 1, \ldots, n_c), \tag{18}$$

where λ_k and $\widetilde{\varphi}_k$ are the eigen-elements of the condensed FE branched model. The k^{th} eigenvector can be partitioned as follows:

$$\widetilde{\varphi}_k = \begin{Bmatrix} {}^c\widetilde{\varphi}_k \\ q \end{Bmatrix} \tag{19}$$

where ${}^c\widetilde{\varphi}_k$ denote the eigenvector of the boundary dof whereas q denote modal generalized coordinates. In order to make the predicted and measured mode shapes' size compatible and also to retain the spectral content of the condensed FE branched model, we propose to insert the q coordinates in the φ_k vector such as:

$$\varphi_k^* = \begin{Bmatrix} \varphi_k \\ q \end{Bmatrix}. \tag{20}$$

So, the condensed energy functional is defined as a function of a composite Rayleigh quotient by combining predicted and measured mode shapes:

$$\mathscr{E}_k\left(\mathrm{x^i}\right) = 1 - \frac{R_k^*}{\omega_k^2}, \tag{21}$$

with

$$R_k^* = \frac{\varphi_k^{*t} K_r \widetilde{\varphi}_k}{\varphi_k^{*t} M_r \widetilde{\varphi}_k}. \tag{22}$$

The identification method is then reduced to the minimization of a global functional $f\left(x^i\right)$, with respect to optimization parameter vector x^i including n parameters, expressed as a function of each component of the vector $\mathscr{E}$:

$$f\left(\mathrm{x^i}\right) = \frac{1}{2}\left\|\mathscr{E}\left(\mathrm{x^i}\right)\right\|^2 = \frac{1}{2}\sum_{k=1}^{m} \mathscr{E}_k^2\left(\mathrm{x^i}\right). \tag{23}$$

The first advantage of this functional is that each term allows the combination of the k^{th} natural frequency and its associated mode shape to from an adimensional term. Thus, as the $\mathscr{E}$ components are the same order, the second advantage of this functional is that weight coefficients are not necessary. To avoid numerical conditioning problems (a 10^{12} ratio between the Young Modulus

and the Poisson ratio), especially for the $J\left(x^i\right)$ Jacobian matrix Eqn. (24), optimization parameters x^i are defined relative to reference values such as the initial values of optimization parameters x^0. This functional is minimized by using the Levenberg-Marquardt algorithm, which is generally acknowledged as very robust and highly efficient in a wide range of problems:

$$\begin{cases} x^0, \mu_0 \text{ given} \\ d_i = -\left(H_i + \mu_i I\right)^{-1} \nabla f\left(x^i\right) \\ x^{i+1} = x^i + \rho_i d_i \end{cases}, \begin{cases} \nabla f\left(x^i\right) = J\left(x^i\right)^T \mathscr{E}\left(x^i\right) \\ H_i \approx J\left(x^i\right)^T J\left(x^i\right). \end{cases} \tag{24}$$

where I and H_i are respectively the identity and the approximate Hessian matrices of size $[n \times n]$. If $\mu_i \to \infty$, the method tends to the steepest descent method, whereas if $\mu_i \to 0$ the method tends to the Gauss-Newton method. Updating damping parameter μ_i is done by calculating a "gain factor", *i.e.* the ratio of the $f\left(x^i\right)$ decrease over the $\mathscr{E}\left(x^i\right)$ decrease, $\mathscr{E}\left(x^i\right)$ vector being expanded with a Taylor series. The descent step ρ_i can be obtained by a "Line Search" algorithm. The method proposed by [22] is used here by setting $\rho_i = 1$ and frequently updating μ_i. This results in smoother performance and faster convergence than that achieved by Marquardt's updating strategy.

Eigen-Derivatives

The Jacobian matrix $J\left(x^i\right)$ (of size $[m \times n]$) of the vector $\mathscr{E}\left(x^i\right)$ implicitly depends on eigen-elements λ_k and $\widetilde{\varphi}_k$ Eqn. (18) of the condensed FE branched model. By taking account of Eqn. (5) for the condensed model and assuming that the eigenvectors are normalized with respect to the condensed mass matrix M_r:

$$\widetilde{\varphi}_k^T M_r \widetilde{\varphi}_k = 1, \left(k = 1, \ldots, m\right). \tag{25}$$

Taking partial derivatives of Eqn. (18) and Eqn. (25) with respect to an optimization parameter x_p yields the following governing equations for eigenvector derivatives [14]:

$$A_k \frac{\partial \widetilde{\varphi}_k}{\partial \mathrm{x_p}} = P_k, \tag{26}$$

and

$$\widetilde{\varphi}_k^T M_r \frac{\partial \widetilde{\varphi}_k}{\partial \mathrm{x_p}} = Q_k \text{ with } Q_k = -\frac{1}{2} \widetilde{\varphi}_k^T \frac{\partial M_r}{\partial \mathrm{x_p}} \widetilde{\varphi}_k, \tag{27}$$

where

$$A_k = \left(K_r - \lambda_k M_r\right), P_k = -\left(\frac{\partial K_r}{\partial \mathrm{x_p}} - \frac{\partial \lambda_k}{\partial \mathrm{x_p}} M_r - \lambda_k \frac{\partial M_r}{\partial \mathrm{x_p}}\right) \widetilde{\varphi}_k. \tag{28}$$

Premultiplying Eqn. (26) by $\widetilde{\varphi}_k^T$ and substituting Eqn. (5) and Eqn. (25), the eigenvalue derivative with respect to x_p is obtained from the relationship:

$$\frac{\partial \lambda_k}{\partial x_p} = \widetilde{\varphi}_k^T \left(\frac{\partial K_r}{\partial x_p} - \lambda_k \frac{\partial M_r}{\partial x_p}\right) \widetilde{\varphi}_k. \tag{29}$$

Concerning the eigenvector derivatives, the problem is that Eqn. (26) is not invertible since the A_k matrix is of rank $(m-1)$. The complete modal method assumes that the k^{th} eigenvector derivative with respect to x_p can be expressed as follows:

$$\frac{\partial \widetilde{\varphi}_k}{\partial \mathrm{x_p}} = \sum_{j=1}^{s} c_j \widetilde{\varphi}_j. \tag{30}$$

Substituting Eqn. (30) and Eqn. (26) and premultiplying by $\widetilde{\varphi}_k^T$ gives:

$$c_j = \frac{\widetilde{\varphi}_j^T \cdot P_k}{\lambda_j - \lambda_k}, j \neq k. \tag{31}$$

Equation (31) shows that the eigenvector derivative has a unique expression (linear combination) in term of all the system eigenvectors, excluding the k^{th} one:

$$\frac{\partial \widetilde{\varphi}_k}{\partial \mathrm{x_p}} = \sum_{\substack{j=1 \\ j \neq k}}^{m} c_j \widetilde{\varphi}_j + c_k \widetilde{\varphi}_k \equiv V_k + c_k \widetilde{\varphi}_k. \tag{32}$$

Substituting Eqn. (32) and Eqn. (27), c_k can be obtained:

$$c_k = Q_k - \widetilde{\varphi}_k M_r V_k. \tag{33}$$

This method is costly in terms of computational time because it requires knowing all the eigenvectors of the system. Thus by substituting Eqn. (32) in Eqn. (26), Ref. [15] proposes removing the singularity of A_k by canceling a component of V_k, Eqn. (26) becomes invertible and a part of the solution V_k is obtained. The complete solution is then given by Eqn. (32) and Eqn. (33). This method requires as many inversions of A_k matrix of size $[m \times m]$ as eigenvector derivatives needed. However, *MGV* rotors are considered as medium systems and the inversion of such matrices is not costly in terms of CPU-time.

Transformation Matrix Derivatives

The partial derivatives of the condensed mass and stiffness matrices with respect to x_p are obtained by differentiating the

transformation matrix ψ Eqn. (13):

$$\frac{\partial \psi}{\partial x_p} = \begin{bmatrix} \frac{\partial \varphi^c}{\partial x_p} & \frac{\partial \varphi^n}{\partial x_p} \\ 0 & 0 \end{bmatrix}, \tag{34}$$

such that $\frac{\partial \varphi^n}{\partial x_p}$ is obtained by applying the Nelson'method in Eqn. (15). By differentiating Eqn. (14), the left arrow of Eqn. (34) can be obtained as shown in Eqn. (35):

$$\frac{\partial \varphi^c}{\partial x_p} = -K_{ii}^{-1} \cdot \left(\frac{\partial K_{ic}}{\partial x_p} - \frac{\partial K_{ii}}{\partial x_p} \varphi^c \right). \tag{35}$$

The partial derivatives of a condensed matrix T_r are then expressed as follows:

$$\frac{\partial T_r}{\partial x_p} = \psi^t \cdot \frac{\partial T}{\partial x_p} \cdot \psi + 2 \cdot \psi^t \cdot T \cdot \frac{\partial \psi}{\partial x_p}, \tag{36}$$

where T can denote the global mass or stiffness matrix.

INDUSTRIAL APPLICATION

The experimental modal analysis was conducted on a *MGV* rotor hanged on a crane via a swivel hoist ring to achieve free-free boundary conditions at best (Fig. 3). The total weight and length of the rotor are 1775 kg and 3.21 m respectively. The hanging rotor was radially excited along a meridian line with an impulse force hammer, a load-cell measuring the transmitted force. A steel impact tip was used to observe a large frequency spectrum. The meridian line was discretized in a fine mesh, a set of 87 measurement points (Fig. 4), for establishing accurate shapes of the measured modes. Module and imaginary part of the successive accelerances obtained with a dynamic analyser permit evaluating the measured natural frequencies and mode shapes.

An identification procedure was performed by updating the FE branched model (Fig. 4) by varying the number of modes m (natural frequencies and associated mode shapes) in the optimization procedure such that m = 4, . . . ,12. A minimum of four modes was retained in order to have sufficient measured modal data such as the dynamics of the studied rotor was preserved. The Poisson ratio was fixed at 0.28, as in [6]. Thus, the optimization problem contains two unknowns:the Young and the shear Moduli of the lamination stack. Initial values of optimization parameters x^0 have been set as follows:

$$\left\{ E_0 = 0.9 \times 10^{11}, G_0 = 0.3 \times 10^{11} \right\}. \tag{37}$$

Figure 5 presents the evolution of the mean global energy functional versus the number of modes m at the end of the convergence. The mean global energy functional is defined as the ratio of $f\left(x^i\right)$ functional (see Eqn. (23)) upon the number of modes

Figure 3. EXPERIMENTAL SETUP.

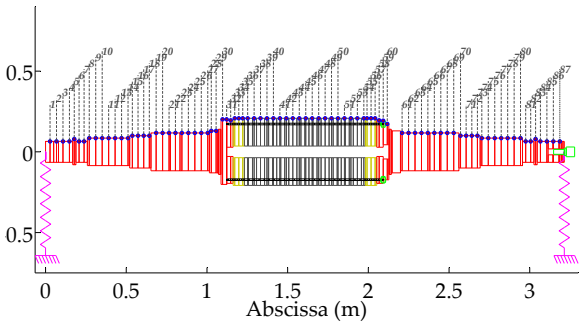

Figure 4. FINITE ELEMENT BRANCHED MODEL. LUMPED MASSES AND TIE RODS ARE PLOTTED IN GREEN AND BLACK RESPECTIVELY WHILE BLUE POINTS REPRESENT MEASUREMENT POINTS.

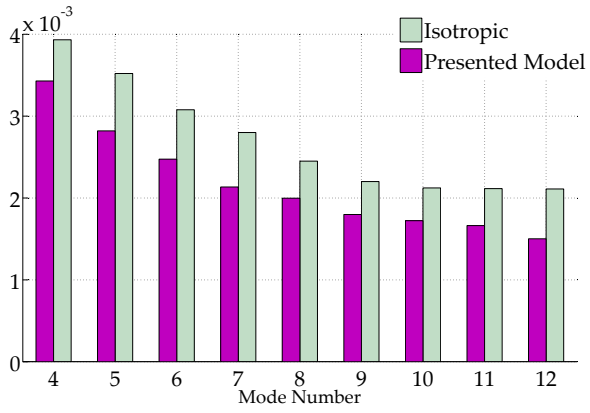

Figure 5. EVOLUTION OF THE MEAN GLOBAL ENERGY FUNCTIONALS VERSUS THE NUMBER OF CONSIDERED MODES.

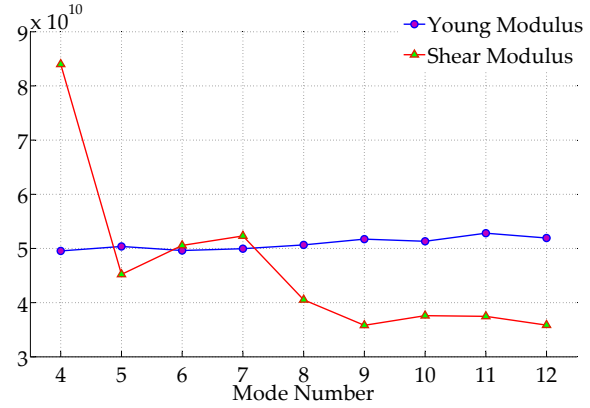

Figure 6. EVOLUTION OF THE YOUNG (CIRCLE) AND SHEAR (TRIANGLE) MODULUI VERSUS THE NUMBER OF CONSIDERED MODES. VALUES ARE PLOTTED IN $N \cdot m^{-2}$.

m. This quantity characterizes the difference between the predicted and measured data for each mode. The mean global energy functional, plotted in dark, decreases with the number of considered modes m which means that the orthotropic model of the lamination stack preserves the dynamics of the studied rotor. The number of considered modes has an influence on the identifies parameters. Figure 6 shows that the identified equivalent constitutive properties of the lamination stack depend on the number of considered modes. However, these constitutive properties tend toward certain asymptotic values from 8 modes. Therefore, it is necessary to take into account a sufficient number of modes, more than 8, to identified relevant parameters. The same identification procedure was performed by considering the lamination stack as an isotropic material, *i.e.* the shear modulus is defined as a linear function of the Young modulus. The mean global energy functional, plotted in light, is around 14% to 40%

Table 1. FIRST TWELVE PREDICTED AND MEASURED LATERAL NATURAL FREQUENCIES.

Index	Measured (Hz)	Predicted (Hz)	Error $(\%)$
1^{st}	173.83	174.33	0.3
2^{nd}	291.02	305.92	5.1
3^{rd}	519.14	529.48	1.9
4^{th}	825.78	771.76	−6.5
5^{th}	996.09	992.13	−0.4
6^{th}	1051.6	1071.7	1.9
7^{th}	1402.7	1384.3	−1.3
8^{th}	1705.1	1732.2	1.6
9^{th}	1932.8	1949.3	0.8
10^{th}	2178.9	2127.0	−2.4
11^{th}	2453.5	2432.5	−0.8
12^{th}	2808.6	2854.5	1.6

higher than the mean global energy functional obtained with the presented model. Morever, the mean global energy functional tends to stabilize if the number of considered modes m is greater than 8 while that of the presented model continues to decrease. Therefore, the identification method presented here is more accurate than classical identification methods considering restrictive assumptions about the mechanical behavior of a lamination stack such as isotropic material. The first twelve predicted and measured natural frequencies are distributed in TAB. 1 while their associated mode shapes are plotted in Fig. 7. It should be noticed that the lateral deflections of the tie rods are not available by the chosen experimental investigation. Moreover, the *MAC* matrix is based only on the lateral deflections of the predicted and measured boundary dof. Thus, the *MAC* matrix does not highlight the tie rods contribution in the global lateral deflections. Consequently, there is a virtual coupling between the 5^{th} and the 6^{th} mode shapes, and also between the 9^{th} and 10^{th} mode shapes. These 6^{th} and 10^{th} the mode shapes are local modes due to the tie rods dynamics. The prediction is obtained by considering 12 modes in the optimization procedure. The relative error between the predicted and measured natural frequencies varies from 0.6% to 6.5% with a mean value equal to 2%. Figure 8 presents a plot of the Modal Assurance Criterion, *i.e.* *MAC* matrix, between predicted and measured mode shapes (see Fig. 7). Figure 7 and Fig. 8 show a good correlation between the predicted and measured mode shapes and also justify the use of the FE branched model and therefore the Craig and Bampton reduction. Indeed,

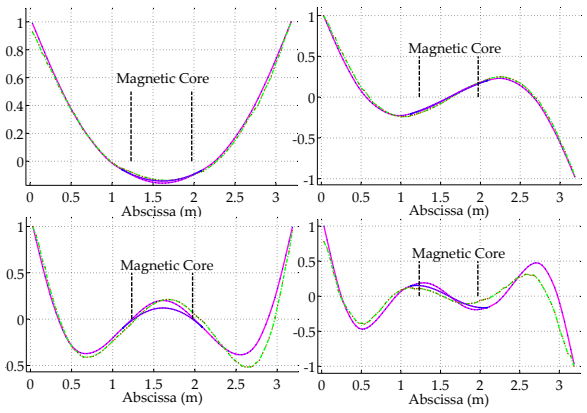

(a) PREDICTED AND MEASURED MODE SHAPES $N°1$ to $N°4$.

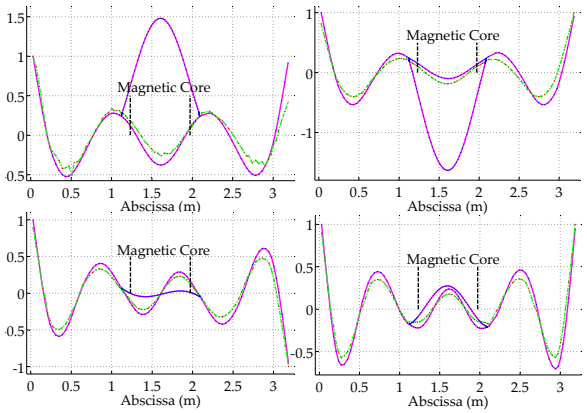

(b) PREDICTED AND MEASURED MODE SHAPES $N°5$ to $N°8$.

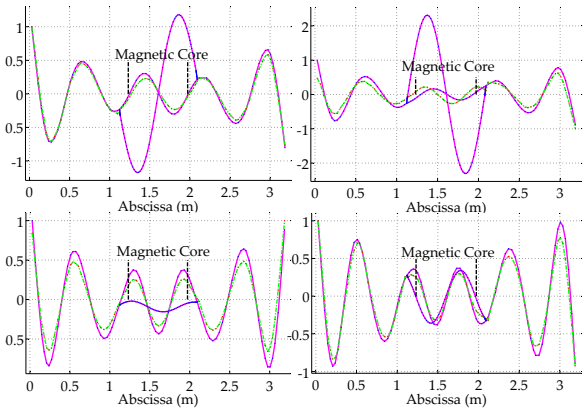

(c) PREDICTED AND MEASURED MODE SHAPES $N°9$ to $N°12$.

Figure 7. FIRST TWELVE PREDICTED (SOLID LINE) AND MEASURED (DASHED LINE) LATERAL MODE SHAPES.

the 6^{th} and 10^{th} modes are local modes mainly due to the tie rods dynamics which could not be observed if the rotor was modeled

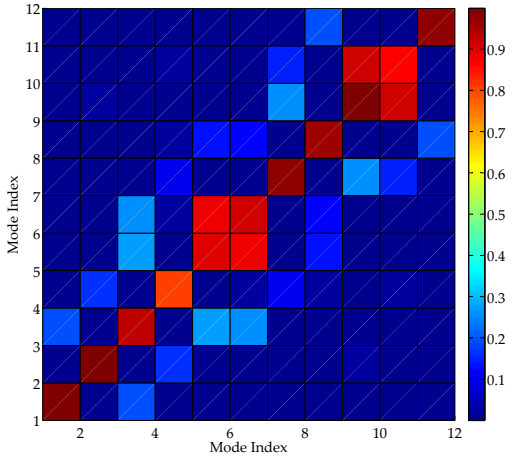

Figure 8. REPRESENTATION OF THE *MAC* MATRIX BETWEEN THE PREDICTED AND MEASURED MODE SHAPES.

with a classical FE model or if a static reduction was used. It proves that the FE branched model is a good way to predict the dynamics of this kind of real assembled structure.

CONCLUSION

The optimization procedure proposed in this paper has been tested on a real industrial induction motor which has a complex design. A finite element branched model was presented by taking into account that *MGV* rotors are assemblies made of different components especially in the magnetic core. Therefore, the prestressed tie rods have been modeled independently of the lamination stack. Moreover, the finite element branched model was able to provide the tie rods modes which have been observed. It is stated that the identified equivalent constitutive properties of the lamination stack depend on the number of considered modes. However, these constitutive properties tend toward certain asymptotic values from eight modes. This identification procedure is very useful for establishing a finite element model based mainly on beam elements containing few dof, which is a great advantage for predicting the rotordynamics, *i.e.* unbalance responses and transient responses. The reliability of such a procedure requires applying it to other induction motors, *i.e. MGV* rotors, in order to predict the dynamic behavior of the *MGV* rotors under development, such as the 30 *MW* range at 6000 *rpm*. This will permit the manufacturer to increase reliability for this range of products.

ACKNOWLEDGMENT

The authors are indebted to Converteam for its support and permission to publish this research.

REFERENCES

[1] Belmans, R., Heylen, W., Vandenput, A., and Geysen, W., 1984. "Influence of rotor-bar stiffness on the critical speed of an induction motor with an aluminium squirrel cage". In IEEE Proceedings, Vol. 131, Part B, N°5, pp. 203–208.

[2] Chang, S., and Lee, D., 2002. "Robust design of a composite air spindle". *Polymer Composites,* **23**(3), pp. 361–371.

[3] McClurg, J., 1987. "Advantages of stiff shaft design on high speed, high horsepower squirrel cage induction motors and generators". In 34th APCI Conference, pp. 259–263.

[4] Ede, J., Howe, D., and Zhu, Z., 2002. "Rotor resonances of high-speed permanent-magnet brushless machines". *IEEE Transactions on Industry Applications,* **38**(6), pp. 1542–1548.

[5] Garvey, S., Penny, J., Friswell, M., and Lees, A., 2004. "The stiffening effect of laminated rotor cores on flexible-rotor electrical machines". In IMechE Event Publications, Vol. 2004, N°2, pp. 193–202.

[6] Chen, Y., Cheng, Y., Liao, J., and Chiou, C., 2008. "Development of a finite element solution module for the analysis of the dynamic behavior and balancing effects of an induction motor system". *Finite Elemens in Analysis and Design*, pp. 2047–2051.

[7] Long, S., Zhu, Z., and Howe, D., 2001. "Vibration behaviour of stators of switched reluctance motors". *IEEE Proceedings: Electric Power Applications,* **148**(3), pp. 257–264.

[8] Tang, Z., Pillay, P., Omekanda, A. M., Li, C., and Cetinkaya, C., 2003. "Effects of material properties on switched reluctance motor vibration determination". In Conference Record - IAS Annual Meeting (IEEE Industry Applications Society), Vol. 1 of *2003 IEEE Industry Applications Conference; 38th IAS Annual Meeting: Crossroads To Innovation*, pp. 235–241.

[9] Garvey, S., 1989. "The vibrational behaviour of laminated components in electrical machines". *Electrical Machines and Drives, 1989. Fourth International Conference on (Conf. Publ. No. ??)*, pp. 226–231.

[10] Kim, Y.-C., and K-W, K., 2006. "Influence of lamination pressure upon the stiffness of laminated rotor". *JSME - International Journal - Series C,* **49**(2), pp. 426–431.

[11] Lee, C., and Kam, T., 2006. "Identification of mechanical properties of elastically restrained laminated composite plates using vibration data". *Journal of Sound and Vibration,* **295**(3-5), pp. 999–1016.

[12] Cugnoni, J., 2005. "Identification par recalage modal et fréquentiel des propriétés constitutives de coques en matériaux composites". Thèse n°3106, Ecole Polytechnique Fédérale de Lausanne.

[13] Feng, X., Zhou, J., and Fan, Y., 2003. "Identifying subregional material parameters of concrete dams using modal data". *Acta Mechanica Solida Sinica,* **16**(1), pp. 88–94.

[14] Ojalvo, I., 1987. "Efficient computation of mode-shape derivatives for large dynamic systems". *AIAA Journal,* **25**(10), pp. 1386–1390.

[15] Nelson, R., 1976. "Simplified calculation of eigenvector derivatives". *AIAA Journal,* **14**(9), pp. 1201–1205.

[16] Min, Y., Zhong-Sheng, L., and Da-Jun, W., 1997. "Comparison of several approximate modal methods for computing mode shape derivatives". *Computers and Structures,* **62**(2), pp. 381–393.

[17] Craig Jr., R., and Bampton, M., 1968. "Coupling of substructures for dynamic analyses". *AIAA Journal,* **6**(7), pp. 1313–1319.

[18] Andrieux, S., and Baranger, T., 2008. "Energy methods for cauchy problems of evolutions equations". *Journal of Physics: Conference Series,* **135**.

[19] Przemieniecki, J.-S., 1985. *Theory of Matrix Structural Analysis*. Dover Publications, INC., New York.

[20] Lalanne, M., and Ferraris, G., 1998. *Rotordynamics Prediction in Engineering*, 2 ed. John Wiley and Sons Ltd, New York.

[21] Cowper, G., 1966. "The shear coefficient in timoshenko's beam theory". *J. of Appl. Mech.,* **33**(2), pp. 335–340.

[22] Nielsen, H., 1999. Damping parameter in marquardt's method. Tech. rep., Technical Univ. of Denmark.